Evidence for WZ and ZZ production in final states with b-tagged jets at CDF

The CDF Higgs Discovery Group

for the CDF Collaboration

March 5, 2012

We present a combined measurement of the production cross section of VZ ($V = W$ or Z) events in final states containing charged leptons (electrons or muons) or neutrinos, and heavy flavor jets, using data collected by the CDF detector at the Fermilab Tevatron Collider. The analyzed samples correspond to 9.45 fb^{-1} of $p\bar{p}$ collisions at $\sqrt{s} = 1.96$ TeV. Assuming the ratio of the production cross sections $\sigma(WZ)$ and $\sigma(ZZ)$ as predicted by the standard model, we measure the total VZ cross section to be $\sigma(VZ) = 4.08\pm^{+1.38}_{-1.26}$ pb. This is consistent with the standard model prediction and corresponds to a significance of about 3.2 standard deviations above the background-only hypothesis.

Preliminary Results for Moriond 2012 Conference

I. INTRODUCTION

The production of VV ($V = W, Z$) boson pairs provides an important test of the electroweak sector of the standard model (SM). In $p\bar{p}$ collisions at $\sqrt{s} = 1.96$ TeV, the next-to-leading order (NLO) SM cross sections for these processes are $\sigma(WW) = 11.3 \pm 0.8$ pb, $\sigma(WZ) = 3.2 \pm 0.2$ pb and $\sigma(ZZ) = 1.2 \pm 0.1$ pb [1]. These cross sections assume both γ^* and Z° components in the neutral current exchange and corresponding production of dilepton final states in the region $75 \leq m_{\ell^+\ell^-} \leq 105$ GeV/c^2. Measuring a significant departure in cross section or deviations in the predicted kinematic distributions would indicate the presence of anomalous gauge boson couplings [2] or new particles in extensions of the SM [3]. The VV production in $p\bar{p}$ collisions at the Fermilab Tevatron Collider has been observed in fully leptonic decay modes [4] and in semi-leptonic decay modes [5], where the combined $WW + WZ$ cross section was measured.

Recently, the DØ experiment presented evidence for WZ and ZZ using the leptonic and fully leptonic decay modes in a b-tagged final state [6]. In this note we report the combination of a set of similar CDF analyses. That is, we report a measurement at CDF of the WZ and ZZ production production cross section in final states where one of the Z bosons decays into $b\bar{b}$ (although there is some signal contribution from $W \to c\bar{s}$, $Z \to c\bar{c}$) and the other weak boson decays to charged leptons or neutrinos ($W \to \ell\nu$, $Z \to \nu\nu$, or $Z \to \ell\ell$, with $\ell = e, \mu$). This analysis is relevant as a proving ground for the search at CDF for a low-mass Higgs boson produced in association with a weak boson and decaying into a $b\bar{b}$ pair [7] since it shares the same selection criteria as well as analysis and combination techniques.

II. SUMMARY OF CONTRIBUTING ANALYSES

This result is the combination of the three CDF analyses [8–10] outlined in Table I. These analyses utilize data corresponding to integrated luminosity of 9.45 fb^{-1}, collected with the CDF [11] detector. They are organized into multiple sub-channels for each different configuration of final state particles. To facilitate proper combination of signals, the analyses were constructed to use mutually exclusive event selections.

In the $\ell\nu b\bar{b}$ analyses [8], events containing an isolated electron or muon, and two or three jets are selected. The presence of a neutrino from the W decay is inferred from a large imbalance of transverse momentum ($\not\!\!E_T$). The $\nu\nu b\bar{b}$ analyses [9] select events containing large $\not\!\!E_T$ and two jets. Finally, in the $\ell\ell b\bar{b}$ analyses [10] events are required to contain two electrons or two muons and at least two jets. Events with two or three jets are analyzed separately. In the $\ell\ell b\bar{b}$ analysis, each lepton flavor of the W/Z boson decay ($\ell = e, \mu$) is treated as an independent channel. In the case of the $\ell\nu b\bar{b}$ analysis lepton types are separated into four different channels based on their purity and location within the detector. To ensure that event samples used for the different analyses do not overlap, the $\ell\nu b\bar{b}$ analyses reject events in which a second isolated electron or muon is identified, and the $\nu\nu b\bar{b}$ analyses reject events in which any isolated electrons or muons are identified.

To isolate the $Z \to b\bar{b}$ decays, algorithms for identifying jets consistent with the decay of a heavy-flavor quark are applied to the jets in each event candidate (b-tagging). The $\ell\nu b\bar{b}$ and $\ell\ell b\bar{b}$ analyses use a multi-variate algorithm (neural network) based on sets of kinematic variables sensitive to displaced decay vertices and tracks within jets with large transverse impact parameters relative to the hard-scatter vertices [12]. A spectrum of increasingly stringent b-tagging operating points is achieved through the implementation of progressively higher requirements on the minimum output of the b-tagging discriminant. Candidate events in the $\ell\nu b\bar{b}$ and $\ell\ell b\bar{b}$ analyses are also separated into channels based on tight and loose tagging definitions. Events with two tight tags (TT), one tight and one loose tag (TL), two loose tags (LL), and a single tight tag (Tx) are used by both analyses. The $\ell\nu b\bar{b}$ analysis also considers events with a single loose tag (Lx). A typical per-jet efficiency and fake rate for the loose (tight) neural network b-tag selection is about 70% (45%) and 7% (0.6%), respectively. The $\nu\nu b\bar{b}$ analysis utilizes a tight b-tagging algorithm [13] based on reconstruction of a displaced secondary vertex and a loose b-tagging algorithm [14] that assigns a likelihood for the tracks within a jet to have originated from a displaced vertex. Based on the output of these algorithms events with two tight tags (SS) and those with one tight tag and one loose tag (SJ) are separated into independent analysis channels. Signal in all of the double-tag samples is primarily composed of events with $Z \to b\bar{b}$ decays but also contains smaller contributions from $Z \to c\bar{c}$ and $W \to c\bar{s}$ decays. In the single-tag samples, which are defined by less stringent requirements on the b-jet content of the event, the contributions from the three decay modes are comparable. All three analyses use multivariate discriminants (MVA) based on neural networks for the final discriminant used for extracting the VZ signal from the backgrounds.

The primary background is from W/Z+jets, and it is modeled with ALPGEN [15] with PYTHIA [16] providing parton-showering and hadronization. The backgrounds from multijet production are measured from control samples in the data. Most backgrounds from other SM processes were generated using PYTHIA. Background rates are normalized either to next-to-leading order (NLO) or higher-order theory calculations or to data control samples. The $\ell\nu b\bar{b}$ analysis normalize the W/Z+jets backgrounds to the data, whereas the $\ell\ell b\bar{b}$ and $\nu\nu b\bar{b}$ analyses normalizes them to

the prediction from ALPGEN. The fraction of the W/Z+jets in which the jets arise from heavy quarks (b or c) is obtained from ALPGEN but is corrected based on a data control region. The background from $t\bar{t}$ events is normalized to the approximate NNLO cross section [17]. The s-channel and t-channel cross sections for the production of single-top quarks are from approximate NNLO+NNLL calculations [18] and approximate NNNLO+NLL calculations [19], respectively.

III. SYSTEMATIC UNCERTAINTIES

Systematic uncertainties differ between analyses, and they affect the rates and shapes of the predicted signal and background templates in correlated ways. The combined result incorporates the sensitivity of predictions to values of nuisance parameters and takes into account correlations in these parameters between analyses. The largest uncertainty contributions and their correlations between are discussed here. Further details are included in the individual analysis notes [8–10].

1. Correlated Systematic Uncertainties

The dominant systematic uncertainties are shown in Appendix Tables II and III for the $\ell\nu b\bar{b}$ channels, in Table IV for the $\nu\nu b\bar{b}$ channels, and in Tables V and VI for the $\ell\ell b\bar{b}$ channels. Each source induces a correlated uncertainty across all CDF channels' signal and background contributions which are sensitive to that source.

The largest uncertainties on signal arise from measured b-tagging efficiencies, jet energy scale, and other Monte Carlo modeling. Shape dependencies of templates on jet energy scale, b-tagging, and gluon radiation ("ISR" and "FSR") are taken into account for some analyses (see tables). The uncertainties on measurements of the integrated luminosities are 5.9% and is correlated between measurements. The three analyses also share the assumed values and uncertainties on the cross sections for WW production and top-quark production processes ($t\bar{t}$ and single top). In most analyses determination of the multijet ("QCD") background involves data control samples, and the methods used differ between analyses. Therefore, there is no assumed correlation in the predicted rates of this background between analysis channels.

Uncertainties on background event rates vary significantly for the different processes. The backgrounds with the largest systematic rate uncertainties are in general quite small. Such uncertainties are constrained through fits to the nuisance parameters and do not affect the result significantly. Since normalizations for the W/Z+heavy flavor backgrounds are obtained from data in the $\ell\nu b\bar{b}$ and $\nu\nu b\bar{b}$ analyses, the corresponding rate uncertainties associated with each analysis are treated as uncorrelated.

IV. MEASUREMENT OF THE $WZ + ZZ$ CROSS SECTION

The total VZ cross section is determined from a fit of the MVA distributions of the background and signal samples to the data. The ratio of the WZ and ZZ cross sections is fixed to its SM prediction. Events from WW production are considered as a background. The fit is performed simultaneously on the distributions in all sub-channels. To check the consistency of the results we perform the fit twice using two statistical methods, a Bayesian calculation and a modified frequentist calculation using $\mathrm{CL_s}$. More details on these methods can be found in Refs. [20, 21].

The combined fit for the total VZ cross section distributions yields $\sigma(VZ) = 4.08\pm^{+1.38}_{-1.26}$ pb. Fig. 1 shows the posterior distribution from the combined cross section fit. This measurement is consistent with the NLO SM prediction of $\sigma(VZ) = 4.4 \pm 0.3$ pb [1]. Based on the measured central value for the VZ cross section and its uncertainties, the significance is estimated to be 3.2 standard deviations (s.d.).

TABLE I: List of analysis channels and their corresponding integrated luminosities. See Sect. II for details ($\ell = e, \mu$).

Channel	Luminosity (fb^{-1})	Reference
$\ell\nu b\bar{b}$, TT/TL/Tx/LL/Lx, 2 jets	9.45	[8]
$\nu\nu b\bar{b}$, SS/SJ, 2/3 jets	9.45	[9]
$\ell\ell b\bar{b}$, TT/TL/Tx/LL, 2/3 jets	9.45	[10]

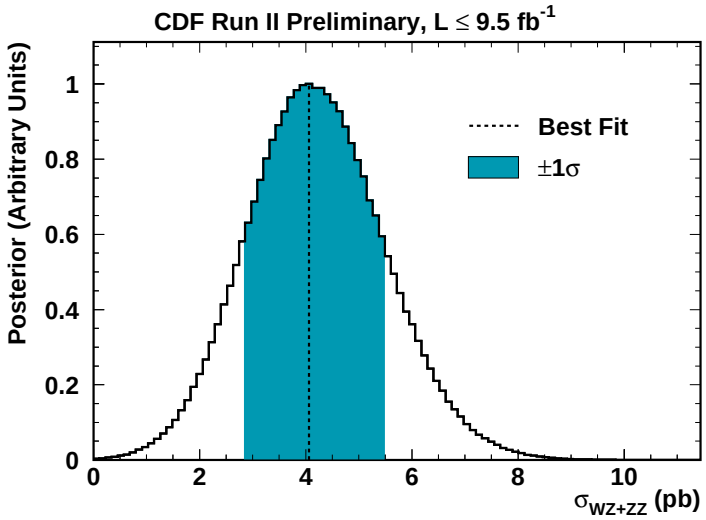

FIG. 1: The posterior curve of the cross section measurement based on the combined fit of the three diboson analyses.

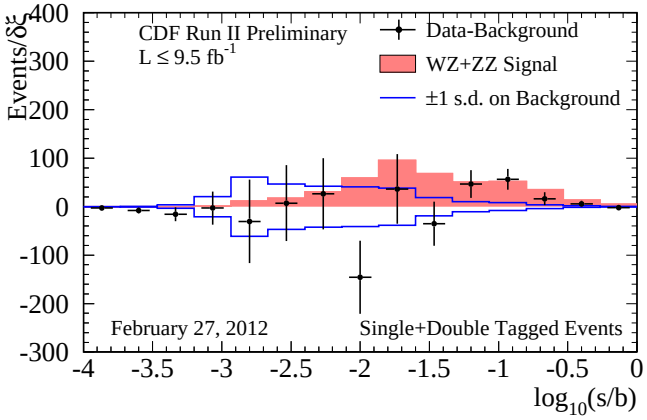

FIG. 2: Comparison of the measured VZ signal (filled histogram) to background-subtracted data (points). The background has been fit to the data in the hypothesis that both signal and background are present. Also shown is the ± 1 standard deviation uncertainty on the fitted background.

To visualize the sensitivity of the combined analysis, we calculate the signal over background (s/b) in each bin of the MVA distributions from the contributing analyses. Bins with similar s/b are then combined to produce a single distribution, shown in Figure 2. In Figure 3 we show the distributions of the invariant mass of the dijet system, summed over all channels, after adjusting the signal and background predictions according to the results of the fit. Figure 4 shows the background subtracted dijet mass distributions after the fit, demonstrating the presence of a hadronic resonance in the data consistent with the SM expectation, both in shape and normalization. Dijet invariant mass plots as wells as the discriminant plots are available in the Appendix (Fig 5 and Fig 6) for the most sensitive tag categories of each analysis.

V. SUMMARY

In summary, we have combined analyses in the $\ell\nu b\bar{b}$, $\nu\nu b\bar{b}$, and $\ell\ell b\bar{b}$ ($\ell = e,\ \mu$) final states from the CDF experiment to observe, with a significance of 3.2 s.d., the production of VZ ($V = W$ or Z) events. The analyzed samples

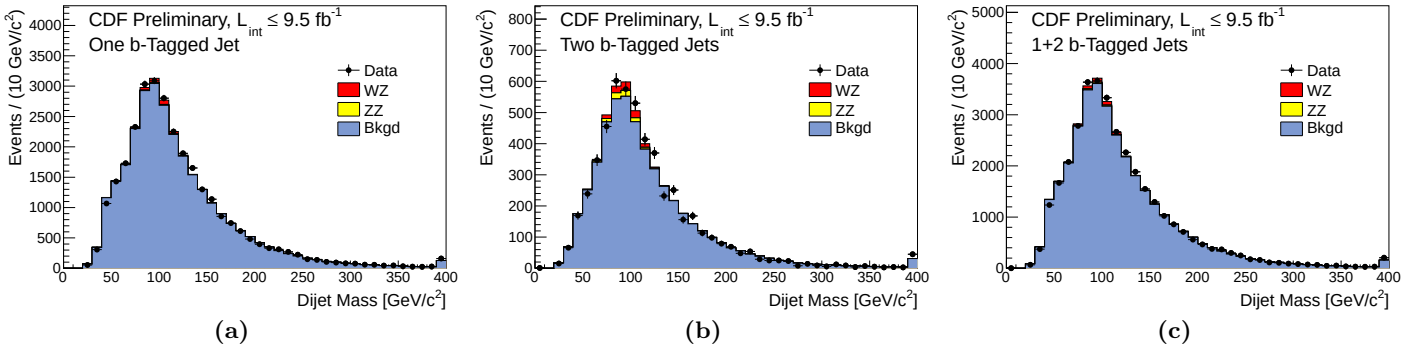

FIG. 3: Comparison of the fitted signal+background to data in the dijet mass distribution (summed over all channels) for the (a) single-tag, and (b) double-tag sub-channels; and (c) the sum of the ST and DT sub-channels. Events with a dijet mass greater than 400 GeV are included in the last bin of the distribution.

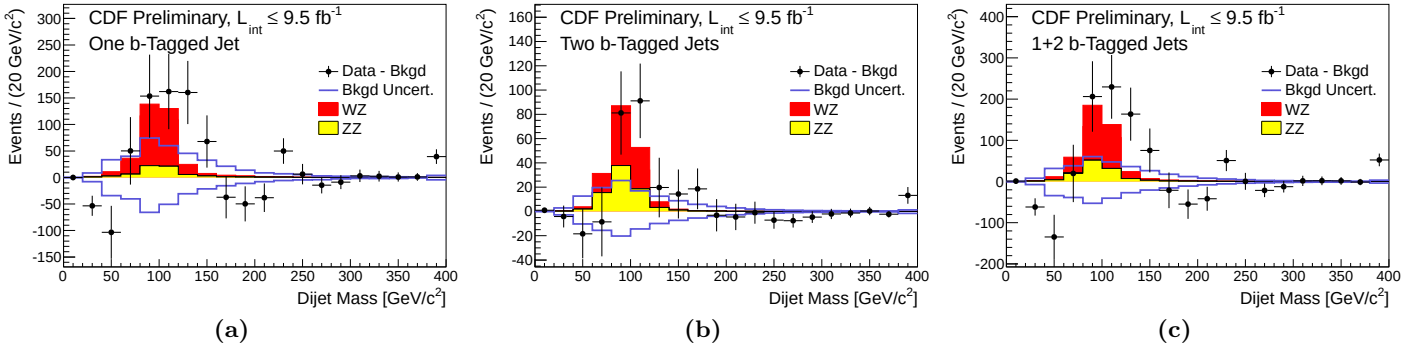

FIG. 4: Comparison of the measured WZ and ZZ signals (filled histograms) to background-subtracted data (points) in the dijet mass distribution (summed over all channels) for the (a) single-tag, and (b) double-tag sub-channels; and (c) the sum of the ST and DT sub-channels. Also shown is the ± 1 standard deviation uncertainty on the fitted background. Events with a dijet mass greater than 400 GeV are included in the last bin of the distribution.

correspond to 9.45 fb^{-1} of $p\bar{p}$ collisions at $\sqrt{s} = 1.96$ TeV. We measure the total cross section for VZ production to be $\sigma(VZ) = 4.08 \pm ^{+1.38}_{-1.26}$ pb. This result demonstrates the ability of the CDF experiment to measure a SM production process with cross section of the same order of magnitude as that expected for Higgs boson production from the same set of background-dominated final states containing two heavy-flavor jets used in our low mass Higgs boson searches.

Acknowledgments

We thank the Fermilab staff and the technical staffs of the participating institutions for their vital contributions. This work was supported by the U.S. Department of Energy and National Science Foundation; the Italian Istituto Nazionale di Fisica Nucleare; the Ministry of Education, Culture, Sports, Science and Technology of Japan; the Natural Sciences and Engineering Research Council of Canada; the National Science Council of the Republic of China; the Swiss National Science Foundation; the A.P. Sloan Foundation; the Bundesministerium für Bildung und Forschung, Germany; the Korean World Class University Program, the National Research Foundation of Korea; the Science and Technology Facilities Council and the Royal Society, UK; the Russian Foundation for Basic Research; the Ministerio de Ciencia e Innovación, and Programa Consolider-Ingenio 2010, Spain; the Slovak R&D Agency; the Academy of Finland; and the Australian Research Council (ARC).

[1] J. M. Campbell and R. K. Ellis, Phys. Rev. D **60**, 113006 (1999) [arXiv:hep-ph/9905386].
[2] K. Hagiwara, S. Ishihara, R. Szalapski, and D. Zeppenfeld, Phys. Rev. D **48** (1993).
[3] J. C. Pati and A. Salam, Phys. Rev. D **10**, 275 (1974); **11** 703(E) (1975);
G. Altarelli, B. Mele, and M. Ruiz-Altaba, Z. Phys. C **45**, 109 (1989); **47**, 676(E) (1990);
L. Randall and R. Sundrum, Phys. Rev. Lett. **83**, 3370 (1999);
H. Davoudiasl, J. L. Hewett, and T. G. Rizzo, Phys. Rev. D **63**, 075004 (2001);
H. He *et al.*, Phys. Rev. D **78**, 031701 (2008).
[4] T. Aaltonen *et al.* (CDF Collaboration), Phys. Rev. Lett. **104**, 201801 (2010);
V. M. Abazov *et al.* (D0 Collaboration), Phys. Lett. B **695**, 67 (2011);
V. M. Abazov *et al.* (D0 Collaboration), Phys. Rev. D **84**, 011103 (2011).
[5] T. Aaltonen *et al.* (CDF Collaboration), Phys. Rev. Lett. **103**, 091803 (2009);
T. Aaltonen *et al.* (CDF Collaboration), Phys. Rev. Lett. **104**, 101801 (2010).
[6] V. M. Abazov *et al.* (D0 Collaboration), DØ Note 6260-CONF (2011).
[7] T. Aaltonen *et al.* (CDF Collaboration), Phys. Rev. Leff **105**, 251802 (2010);
T. Aaltonen *et al.* (CDF Collaboration), Phys. Rev. Leff **103**, 101802 (2009);
T. Aaltonen *et al.* (CDF Collaboration), Phys. Rev. Leff **104**, 141801 (2010).
[8] T. Aaltonen *et al.* (CDF Collaboration), CDF Conference Note 10796 (2012).
[9] T. Aaltonen *et al.* (CDF Collaboration), CDF Conference Note 10798 (2012).
[10] T. Aaltonen *et al.* (CDF Collaboration), CDF Conference Note 10799 (2012).
[11] D. Acosta *et al.* (CDF Collaboration), Phys. Rev. D **71**, 032001 (2005) [hep-ex/0412071].
[12] T. Aaltonen *et al.* (CDF Collaboration), CDF Conference Note 10803 (2012).
[13] D. Acosta *et al.* (CDF Collaboration), Phys. Rev. D **71**, 052003 (2005) [hep-ex/0410041].
[14] A. Abulencia *et al.* (CDF and CDF - Run II Collaborations), Phys. Rev. D **74**, 072006 (2006) [hep-ex/0607035].
[15] M. L. Mangano, M. Moretti, F. Piccinini, R. Pittau and A. D. Polosa, JHEP **0307**, 001 (2003). [arXiv:hep-ph/0206293].
[16] T. Sjöstrand, L. Lonnblad and S. Mrenna, arXiv:hep-ph/0108264.
[17] U. Langenfeld, S. Moch and P. Uwer, Phys. Rev. D **80**, 054009 (2009) [arXiv:0906.5273 [hep-ph]].
[18] N. Kidonakis, arXiv:1005.3330 [hep-ph] (2010);
N. Kidonakis, Phys. Rev. D **81**, 054028 (2010).
[19] N. Kidonakis, Phys. Rev. D **74**, 114012 (2006) [arXiv:hep-ph/0609287].
[20] T. Junk, Nucl. Instrum. Methods A **434**, 435 (1999);
A. L. Read, J. Phys. G **28**, 2693 (2002).
[21] W. Fisher, FERMILAB-TM-2386-E (2006).

APPENDIX A: ADDITIONAL MATERIAL

TABLE II: Systematic uncertainties for the CDF $\ell\nu b\bar{b}$ single tight tag (Tx) and single loose tag (Lx) channels. Systematic uncertainties are listed by name; see the original references for a detailed explanation of their meaning and on how they are derived. Uncertainties are relative, in percent on the event yield. Shape uncertainties are labeled with an "(S)".

CDF $\ell\nu b\bar{b}$ single tight tag (Tx) channels relative uncertainties (%)

Contribution	W+HF	Mistags	Top	Diboson	Non-W	WH
Luminosity ($\sigma_{\text{inel}}(p\bar{p})$)	3.8	0	3.8	3.8	0	3.8
Luminosity Monitor	4.4	0	4.4	4.4	0	4.4
Lepton ID	2.0-4.5	0	2.0-4.5	2.0-4.5	0	2.0-4.5
Jet Energy Scale	3.2-6.9(S)	0.9-1.8(S)	0.8-9.7(S)	3.6-13.2(S)	0	3.0-5.0(S)
Mistag Rate (tight)	0	19	0	0	0	0
Mistag Rate (loose)	0	0	0	0	0	0
B-Tag Efficiency (tight)	0	0	3.9	3.9	0	3.9
B-Tag Efficiency (loose)	0	0	0	0	0	0
$t\bar{t}$ Cross Section	0	0	10	0	0	0
Diboson Rate	0	0	0	6.0	0	0
Signal Cross Section	0	0	0	0	0	5
HF Fraction in W+jets	30	0	0	0	0	0
ISR+FSR+PDF	0	0	0	0	0	3.8-6.8
Q^2	3.2-6.9(S)	0.9-1.8(S)	0	0	0	0
QCD Rate	0	0	0	0	40	0

CDF $\ell\nu b\bar{b}$ single loose tag (Lx) channels relative uncertainties (%)

Contribution	W+HF	Mistags	Top	Diboson	Non-W	WH
Luminosity ($\sigma_{\text{inel}}(p\bar{p})$)	3.8	0	3.8	3.8	0	3.8
Luminosity Monitor	4.4	0	4.4	4.4	0	4.4
Lepton ID	2	0	2	2	0	2
Jet Energy Scale	2.2-6.0(S)	0.9-1.8(S)	1.6-8.6(S)	4.6-9.6(S)	0	3.1-4.8(S)
Mistag Rate (tight)	0	0	0	0	0	0
Mistag Rate (loose)	0	10	0	0	0	0
B-Tag Efficiency (tight)	0	0	0	0	0	0
B-Tag Efficiency (loose)	0	0	3.2	3.2	0	3.2
$t\bar{t}$ Cross Section	0	0	10	0	0	0
Diboson Rate	0	0	0	6.0	0	0
Signal Cross Section	0	0	0	0	0	10
HF Fraction in W+jets	30	0	0	0	0	0
ISR+FSR+PDF	0	0	0	0	0	2.4-4.9
QCD Rate	2.1-6.0(S)	0.9-1.8(S)	0	0	40	0

TABLE III: Systematic uncertainties for the CDF $\ell\nu b\bar{b}$ double tight tag (TT), one tight tag and one loose tag (TL) and double loose tag (LL) channels. Systematic uncertainties are listed by name; see the original references for a detailed explanation of their meaning and on how they are derived. Uncertainties are relative, in percent on the event yield. Shape uncertainties are labeled with an "(S)".

CDF $\ell\nu b\bar{b}$ double tight tag (TT) channels relative uncertainties (%)

Contribution	W+HF	Mistags	Top	Diboson	Non-W	WH
Luminosity ($\sigma_{\rm inel}(p\bar{p})$)	3.8	0	3.8	3.8	0	3.8
Luminosity Monitor	4.4	0	4.4	4.4	0	4.4
Lepton ID	2.0-4.5	0	2.0-4.5	2.0-4.5	0	2.0-4.5
Jet Energy Scale	4.0-16.6(S)	0.9-3.3(S)	0.9-10.4(S)	4.7-19.7(S)	0	2.3-13.6(S)
Mistag Rate (tight)	0	40	0	0	0	0
Mistag Rate (loose)	0	0	0	0	0	0
B-Tag Efficiency (tight)	0	0	7.8	7.8	0	7.8
B-Tag Efficiency (loose)	0	0	0	0	0	0
$t\bar{t}$ Cross Section	0	0	10	0	0	0
Diboson Rate	0	0	0	6.0	0	0
Signal Cross Section	0	0	0	0	0	5
HF Fraction in W+jets	30	0	0	0	0	0
ISR+FSR+PDF	0	0	0	0	0	6.4-12.6
Q^2	4.0-8.8(S)	0.9-1.8(S)	0	0	0	0
QCD Rate	0	0	0	0	40	0

CDF $\ell\nu b\bar{b}$ one tight and one loose tag (TL) channels relative uncertainties (%)

Contribution	W+HF	Mistags	Top	Diboson	Non-W	WH
Luminosity ($\sigma_{\rm inel}(p\bar{p})$)	3.8	0	3.8	3.8	0	3.8
Luminosity Monitor	4.4	0	4.4	4.4	0	4.4
Lepton ID	2.0-4.5	0	2.0-4.5	2.0-4.5	0	2.0-4.5
Jet Energy Scale	3.9-12.4(S)	0.9-3.3(S)	1.4-11.5(S)	5.0-16.0(S)		2.5-16.1(S)
Mistag Rate (tight)	0	19	0	0	0	0
Mistag Rate (loose)	0	10	0	0	0	0
B-Tag Efficiency (tight)	0	0	3.9	3.9	0	3.9
B-Tag Efficiency (loose)	0	0	3.2	3.2	0	3.2
$t\bar{t}$ Cross Section	0	0	10	0	0	0
Diboson Rate	0	0	0	6.0	0	0
Signal Cross Section	0	0	0	0	0	5
HF Fraction in W+jets	30	0	0	0	0	0
ISR+FSR+PDF	0	0	0	0	0	3.3-10.3
Q^2	3.9-7.7(S)	0.9-1.9(S)	0	0	0	0
QCD Rate	0	0	0	0	40	0

CDF $\ell\nu b\bar{b}$ one tight and one loose tag (TL) channels relative uncertainties (%)

Contribution	W+HF	Mistags	Top	Diboson	Non-W	WH
Luminosity ($\sigma_{\rm inel}(p\bar{p})$)	3.8	0	3.8	3.8	0	3.8
Luminosity Monitor	4.4	0	4.4	4.4	0	4.4
Lepton ID	2	0	2	2	0	2
Jet Energy Scale	3.6-6.9(S)	0.9-1.8(S)	1.7-7.9(S)	1.2-8.5	0	2.7-5.4(S)
Mistag Rate (tight)	0	0	0	0	0	0
Mistag Rate (loose)	0	20	0	0	0	0
B-Tag Efficiency (tight)	0	0	0	0	0	0
B-Tag Efficiency (loose)	0	0	6.3	6.3	0	6.3
$t\bar{t}$ Cross Section	0	0	10	0	0	0
Diboson Rate	0	0	0	6.0	0	0
Signal Cross Section	0	0	0	0	0	10
HF Fraction in W+jets	30	0	0	0	0	0
ISR+FSR+PDF	0	0	0	0	0	2.0-13.6
QCD Rate	3.6-6.9(S)	0.9-1.8(S)	0	0	40	0

TABLE IV: Systematic uncertainties for the CDF $\nu\nu b\bar{b}$ tight double tag (SS) and loose double tag (SJ) channels. Systematic uncertainties are listed by name; see the original references for a detailed explanation of their meaning and on how they are derived. Uncertainties are relative, in percent on the event yield. Shape uncertainties are labeled with an "(S)".

CDF $\nu\nu b\bar{b}$ tight double tag (SS) channel relative uncertainties (%)

Contribution	ZH	WH	Multijet	Mistags	Top Pair	S. Top	Diboson	W + HF	Z + HF
Luminosity	3.8	3.8			3.8	3.8	3.8	3.8	3.8
Lumi Monitor	4.4	4.4			4.4	4.4	4.4	4.4	4.4
Tagging SF	10.4	10.4			10.4	10.4	10.4	10.4	10.4
Trigger Eff. (S)	0.9	1.4	0.9		0.9	1.6	2.0	1.8	1.2
Lepton Veto	2.0	2.0			2.0	2.0	2.0	2.0	2.0
PDF Acceptance	3.0	3.0			3.0	3.0	3.0	3.0	3.0
JES (S)	$^{+1.7}_{-1.8}$	$^{+2.4}_{-2.3}$			$^{+0.0}_{-0.1}$	$^{+2.5}_{-2.4}$	$^{+4.1}_{-4.5}$	$^{+4.3}_{-4.6}$	$^{+8.8}_{-3.2}$
ISR/FSR	$^{+3.0}_{+3.0}$								
Cross-Section	5	5			10	10	6	30	30
Multijet Norm. (shape)			2.5						
Mistag (S)				$^{+36.7}_{-30}$					

CDF $\nu\nu b\bar{b}$ loose double tag (SJ) channel relative uncertainties (%)

Contribution	ZH	WH	Multijet	Mistags	Top Pair	S. Top	Diboson	W + HF	Z + HF
Luminosity	3.8	3.8			3.8	3.8	3.8	3.8	3.8
Lumi Monitor	4.4	4.4			4.4	4.4	4.4	4.4	4.4
Tagging SF	8.3	8.3			8.3	8.3	8.3	8.3	8.3
Trigger Eff. (S)	1.2	1.7	1.6		0.9	1.8	2.0	2.5	1.9
Lepton Veto	2.0	2.0			2.0	2.0	2.0	2.0	2.0
PDF Acceptance	3.0	3.0			3.0	3.0	3.0	3.0	3.0
JES (S)	$^{+1.9}_{-1.9}$	$^{+2.4}_{-2.4}$			$^{+3.0}_{-2.8}$	$^{-0.6}_{0.2}$	$^{+4.2}_{-4.2}$	$^{+6.8}_{-5.9}$	$^{+8.3}_{-3.1}$
ISR/FSR	$^{+2.4}_{-2.4}$								
Cross-Section	5.0	5.0			10	10	6	30	30
Multijet Norm.			1.6						
Mistag (S)				$^{+65.2}_{-38.5}$					

TABLE V: Systematic uncertainties for the CDF $\ell\ell b\bar{b}$ single tight tag (Tx) and double loose tag (LL) channels. Systematic uncertainties are listed by name; see the original references for a detailed explanation of their meaning and on how they are derived. Uncertainties are relative, in percent on the event yield. Shape uncertainties are labeled with an "(S)".

CDF $\ell\ell b\bar{b}$ single tight tag (TT) channels relative uncertainties (%)

Contribution	Fakes	$t\bar{t}$	WW	WZ	ZZ	$Z+c\bar{c}$	$Z+b\bar{b}$	Mistags	ZH
Luminosity ($\sigma_{\rm inel}(p\bar{p})$)		3.8	3.8	3.8	3.8	3.8	3.8		3.8
Luminosity Monitor		4.4	4.4	4.4	4.4	4.4	4.4		4.4
Lepton ID		1	1	1	1	1	1		1
Lepton Energy Scale		1.5	1.5	1.5	1.5	1.5	1.5		1.5
Fake $Z\to e^+e^-$	50								
Fake $Z\to \mu^+\mu^-$	5								
Tight Mistag Rate								19	
Loose Mistag Rate									
JES [e^+e^-, 2 jet]		$^{-0.3}_{+0.3}$	$^{+13.7}_{-13.5}$	$^{+8.5}_{-8.5}$	$^{+6.5}_{-6.3}$	$^{+13.2}_{-13.2}$	$^{+11.0}_{-11.1}$	$^{+12.0}_{-12.0}$	$^{+3.5}_{-3.8}$
JES [e^+e^-, 3 jet]		$^{+7.1}_{-7.1}$	$^{+8.9}_{-8.2}$	$^{+17.0}_{-17.0}$	$^{+15.4}_{-15.4}$	$^{+16.4}_{-16.4}$	$^{+15.8}_{-15.9}$	$^{+18.6}_{-18.5}$	$^{+15.4}_{-15.7}$
JES [$\mu^+\mu^-$, 2 jet]		$^{+0.6}_{-0.7}$	$^{+3.9}_{-3.3}$	$^{+8.6}_{-8.6}$	$^{+7.6}_{-7.7}$	$^{+10.2}_{-10.5}$	$^{+9.3}_{-9.3}$	$^{+11.1}_{-11.1}$	$^{+3.4}_{-3.7}$
JES [$\mu^+\mu^-$, 3 jet]		$^{+5.5}_{-5.5}$	$^{+5.7}_{-1.9}$	$^{+16.6}_{-16.6}$	$^{+16.8}_{-16.8}$	$^{+16.1}_{-16.2}$	$^{+16.1}_{-16.2}$	$^{+17.5}_{-17.5}$	$^{+13.8}_{-13.9}$
Tight b-tag Rate		3.9	3.9	3.9	3.9	3.9	3.9		3.9
Loose b-tag Rate									
$t\bar{t}$ Cross Section		10							
Diboson Cross Section			6	6	6				
Z+HF Cross Section						40	40		
ZH Cross Section									5
ISR/FSR									0.9–12.8
Electron Trigger Eff.		1	1	1	1	1	1		1
Muon Trigger Eff.		5	5	5	5	5	5		5

CDF $\ell\ell b\bar{b}$ double loose tag (LL) channels relative uncertainties (%)

Contribution	Fakes	$t\bar{t}$	WW	WZ	ZZ	$Z+c\bar{c}$	$Z+b\bar{b}$	Mistags	ZH
Luminosity ($\sigma_{\rm inel}(p\bar{p})$)		3.8	3.8	3.8	3.8	3.8	3.8		3.8
Luminosity Monitor		4.4	4.4	4.4	4.4	4.4	4.4		4.4
Lepton ID		1	1	1	1	1	1		1
Lepton Energy Scale		1.5	1.5	1.5	1.5	1.5	1.5		1.5
Fake $Z\to e^+e^-$	50								
Fake $Z\to \mu^+\mu^-$	5								
Tight Mistag Rate									
Loose Mistag Rate								20	
JES [e^+e^-, 2 jet]		$^{+0.5}_{-0.5}$	$^{+7.5}_{-4.8}$	$^{+8.6}_{-8.7}$	$^{+9.0}_{-8.9}$	$^{+10.0}_{-9.3}$	$^{+11.3}_{-11.0}$	$^{+12.5}_{-12.5}$	$^{+4.0}_{-4.4}$
JES [e^+e^-, 3 jet]		$^{+8.6}_{-8.6}$	$^{+32.9}_{-29.5}$	$^{+14.6}_{-14.9}$	$^{+16.5}_{-15.2}$	$^{+20.8}_{-20.8}$	$^{+17.8}_{-17.9}$	$^{+18.9}_{-19.0}$	$^{+14.6}_{-15.4}$
JES [$\mu^+\mu^-$, 2 jet]		$^{+2.5}_{-2.5}$	$^{+4.5}_{-3.0}$	$^{+6.7}_{-6.7}$	$^{+10.2}_{-9.9}$	$^{+9.2}_{-9.3}$	$^{+7.7}_{-7.6}$	$^{+11.5}_{-11.5}$	$^{+3.9}_{-4.3}$
JES [$\mu^+\mu^-$, 3 jet]		$^{+9.2}_{-9.2}$	$^{+13.4}_{-10.4}$	$^{+14.1}_{-14.1}$	$^{+16.6}_{-16.6}$	$^{+14.7}_{-14.7}$	$^{+16.8}_{-16.9}$	$^{+17.5}_{-17.5}$	$^{+11.6}_{-12.2}$
Tight b-tag Rate									
Loose b-tag Rate		6.3	6.3	6.3	6.3	6.3	6.3		6.3
$t\bar{t}$ Cross Section		10							
Diboson Cross Section			6	6	6				
Z+HF Cross Section						40	40		
ZH Cross Section									5
ISR/FSR									3.1–15.2
Electron Trigger Eff.		1	1	1	1	1	1		1
Muon Trigger Eff.		5	5	5	5	5	5		5

TABLE VI: Systematic uncertainties for the CDF $\ell\ell b\bar{b}$ tight double tag (TT) and one tight tag and one loose tag (TL) channels. Systematic uncertainties are listed by name; see the original references for a detailed explanation of their meaning and on how they are derived. Uncertainties are relative, in percent on the event yield. Shape uncertainties are labeled with an "(S)".

CDF $\ell\ell b\bar{b}$ tight double tag (TT) channels relative uncertainties (%)

Contribution	Fakes	$t\bar{t}$	WW	WZ	ZZ	$Z+c\bar{c}$	$Z+b\bar{b}$	Mistags	ZH
Luminosity ($\sigma_{\rm inel}(p\bar{p})$)		3.8	3.8	3.8	3.8	3.8	3.8		3.8
Luminosity Monitor		4.4	4.4	4.4	4.4	4.4	4.4		4.4
Lepton ID		1	1	1	1	1	1		1
Lepton Energy Scale		1.5	1.5	1.5	1.5	1.5	1.5		1.5
Fake $Z\to e^+e^-$	50								
Fake $Z\to \mu^+\mu^-$	5								
Tight Mistag Rate								40	
Loose Mistag Rate									
JES [e^+e^-, 2 jet]		$^{+0.8}_{-0.7}$	$^{+14.4}_{-13.2}$	$^{+6.2}_{-6.2}$	$^{+8.2}_{-8.3}$	$^{+5.6}_{-5.6}$	$^{+8.1}_{-7.9}$	$^{+10.4}_{-10.4}$	$^{+3.6}_{-4.2}$
JES [e^+e^-, 3 jet]		$^{+8.3}_{-8.2}$	$^{-0.7}_{+1.7}$	$^{-4.2}_{+4.3}$	$^{+14.4}_{-13.3}$	$^{+10.6}_{-10.5}$	$^{+13.2}_{-13.2}$	$^{+12.4}_{-12.4}$	$^{+15.1}_{-14.9}$
JES [$\mu^+\mu^-$, 2 jet]		$^{+1.0}_{-0.9}$	$^{+5.4}_{+2.1}$	$^{+13.4}_{-13.4}$	$^{+7.7}_{-7.7}$	$^{-1.5}_{+1.5}$	$^{+8.2}_{-8.2}$	$^{+5.7}_{-5.8}$	$^{+3.1}_{-3.5}$
JES [$\mu^+\mu^-$, 3 jet]		$^{+9.3}_{-9.1}$	$^{+3.9}_{-3.0}$	$^{+4.8}_{-5.7}$	$^{+15.5}_{-15.5}$	$^{+7.3}_{-7.3}$	$^{+14.2}_{-14.5}$	$^{+20.5}_{-18.0}$	$^{+12.5}_{-13.3}$
Tight b-tag Rate		7.8	7.8	7.8	7.8	7.8	7.8		7.8
Loose b-tag Rate									
$t\bar{t}$ Cross Section		10							
Diboson Cross Section			6	6	6				
Z+HF Cross Section						40	40		
ZH Cross Section									5
ISR/FSR									5.5–7.6
Electron Trigger Eff.		1	1	1	1	1	1		1
Muon Trigger Eff.		5	5	5	5	5	5		5

CDF $\ell\ell b\bar{b}$ one tight and one loose tag (TL) channels relative uncertainties (%)

Contribution	Fakes	$t\bar{t}$	WW	WZ	ZZ	$Z+c\bar{c}$	$Z+b\bar{b}$	Mistags	ZH
Luminosity ($\sigma_{\rm inel}(p\bar{p})$)		3.8	3.8	3.8	3.8	3.8	3.8		3.8
Luminosity Monitor		4.4	4.4	4.4	4.4	4.4	4.4		4.4
Lepton ID		1	1	1	1	1	1		1
Lepton Energy Scale		1.5	1.5	1.5	1.5	1.5	1.5		1.5
Fake $Z\to e^+e^-$	50								
Fake $Z\to \mu^+\mu^-$	5								
Tight Mistag Rate								19	
Loose Mistag Rate								10	
JES [e^+e^-, 2 jet]		$^{+0.9}_{-1.0}$	$^{+13.0}_{-12.6}$	$^{+9.3}_{-9.4}$	$^{+10.3}_{-10.2}$	$^{+10.3}_{-10.3}$	$^{+8.9}_{-9.3}$	$^{+10.4}_{-10.4}$	$^{+4.0}_{-4.2}$
JES [e^+e^-, 3 jet]		$^{+6.9}_{-7.0}$	$^{+10.3}_{-8.3}$	$^{+16.2}_{-16.0}$	$^{+14.6}_{-14.5}$	$^{+22.8}_{-23.4}$	$^{+15.1}_{-15.2}$	$^{+18.5}_{-18.5}$	$^{+14.3}_{-14.4}$
JES [$\mu^+\mu^-$, 2 jet]		$^{+1.1}_{-1.1}$	$^{+3.7}_{1.8}$	$^{+6.5}_{-6.5}$	$^{+7.5}_{-7.5}$	$^{+12.5}_{-12.4}$	$^{+10.1}_{-10.1}$	$^{+11.0}_{-11.0}$	$^{+4.0}_{-4.1}$
JES [$\mu^+\mu^-$, 3 jet]		$^{+8.0}_{-8.0}$	$^{+2.0}_{-1.6}$	$^{+14.4}_{-14.5}$	$^{+24.1}_{-24.1}$	$^{+16.0}_{-14.7}$	$^{+17.5}_{-17.6}$	$^{+14.3}_{-14.2}$	$^{+13.1}_{-14.0}$
Tight b-tag Rate		3.9	3.9	3.9	3.9	3.9	3.9		3.9
Loose b-tag Rate		3.2	3.2	3.2	3.2	3.2	3.2		3.2
$t\bar{t}$ Cross Section		10							
Diboson Cross Section			6	6	6				
Z+HF Cross Section						40	40		
ZH Cross Section									5
ISR/FSR									3.4–7.0
Electron Trigger Eff.		1	1	1	1	1	1		1
Muon Trigger Eff.		5	5	5	5	5	5		5

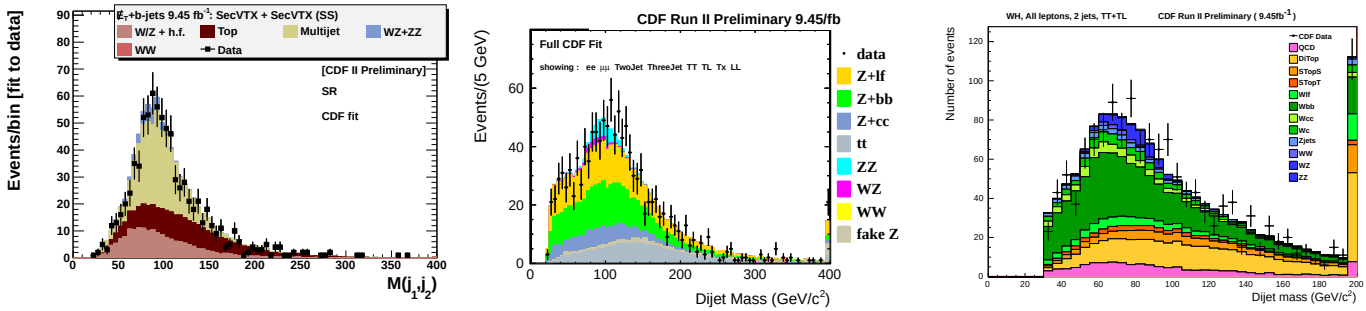

(a) (b) (c)

FIG. 5: Comparison of the fitted signal+background to data in the dijet mass distribution for each channel (a) $\nu\nu b\bar{b}$ for double-tight-tag events (b) $\ell\ell b\bar{b}$ for all tag categories combined; and (c) $\ell\nu b\bar{b}$ TT and TL combined.

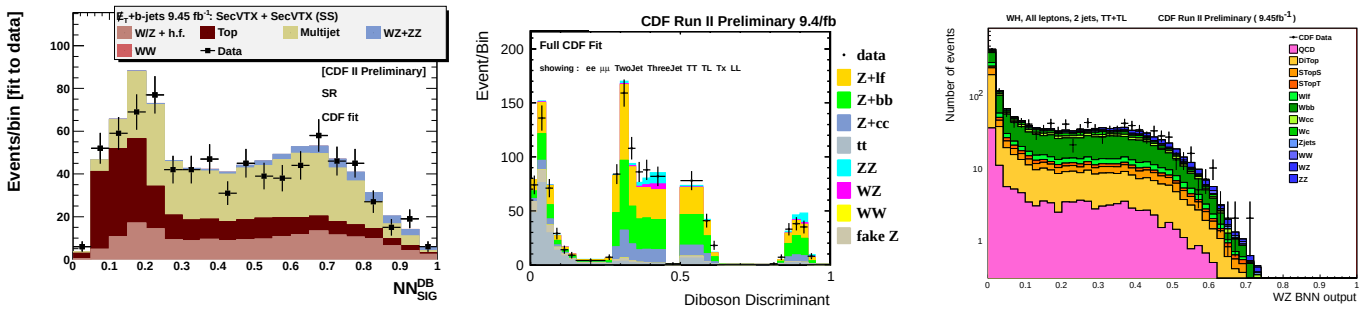

(a) (b) (c)

FIG. 6: Comparison of the fitted signal+background to data in the final discriminant distribution for each channel (a) $\nu\nu b\bar{b}$ for double-tight-tag events (b) $\ell\ell b\bar{b}$ for all tag categories combined; and (c) $\ell\nu b\bar{b}$ TT and TL combined.